

Towards a Clinically Optimized Tilt Mechanism for Bilateral Micromanipulation with Steady-Hand Eye Robot*

Robert Roth, *Student Member, IEEE*, Jiahao Wu, *Student Member, IEEE*, Alireza Alamdar, Russell H. Taylor, *Life Fellow, IEEE*, Peter Gehlbach, *Member, IEEE*
and Iulian Iordachita, *Senior Member, IEEE*

Abstract— Cooperative robotic systems for vitreoretinal surgery can enable novel surgical approaches by allowing the surgeon to perform procedures with enhanced stabilization and high accuracy tool movements. This paper presents the optimization and design of a four-bar linkage type tilt mechanism for a novel Steady-Hand Eye Robot (SHER) which can be used equivalently on both, the left and right patient side, during a bilateral approach with two robots. In this optimization, it is desirable to limit the workspace needed for compensation motions that ensure a virtual remote center of motion (V-RCM). The safety space around the patient, the space for the surgeon's hand and maintaining positional accuracy are also included in the optimization. The applicability of the resulting optimized mechanism was confirmed with a design prototype in a representative mock-up of the surgical setting allowing multiple directions of robot approach towards a medical phantom.

I. INTRODUCTION

Vitreoretinal micro-surgery requires high surgical accuracy and precision for surgeons, mainly due to the extremely small diameter of retinal vessels ($< 130 \mu\text{m}$ [1]) and the very thin and fragile retina ($100\text{-}300 \mu\text{m}$ [2]). Moreover, the surgeon's physiological hand tremor ($> 100 \mu\text{m}$ [3]) may prevent completion of the procedure and, on occasion, cause unsatisfactory surgical results. To solve the above issues, researchers have developed a number of robotic systems to help surgeons perform more stable and precise vitreoretinal surgery.

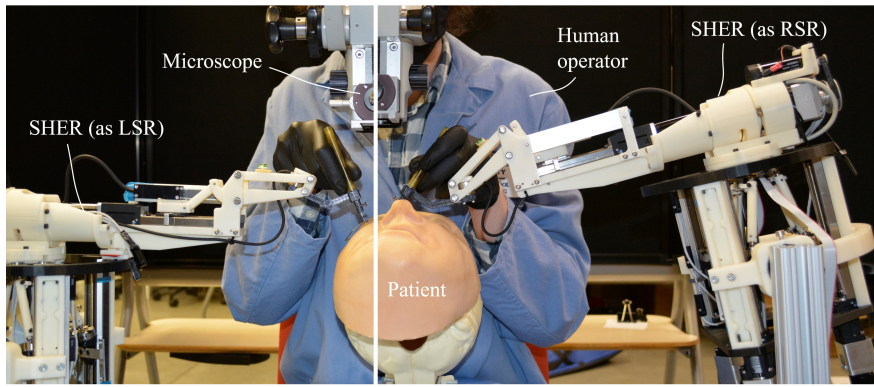


Figure 1. Demonstration of bilateral setup with the new SHER prototype (Left, combination image), Degrees of freedom of new SHER system (right)

*Research supported by U.S. National Institutes of Health under grant number 1R01EB025883-01A1 and JHU internal funds.

R. Roth is with the Technical University of Munich, Germany and with LCSR at the Johns Hopkins University, Baltimore, MD 21218 USA (corresponding author to provide phone: +49-157-515-07220; e-mail: robert.roth@tum.de).

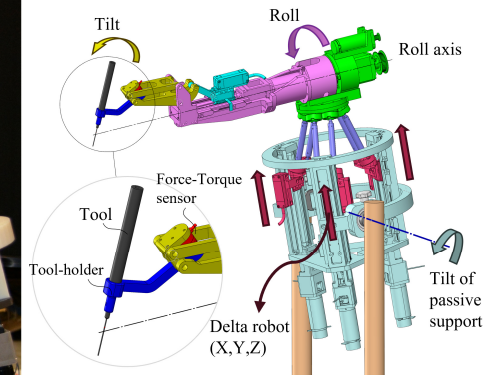
J. Wu is with the T Stone Robotics Institute, the Department of Mechanical and Automation Engineering, The Chinese University of Hong Kong, HKSAR, and with LCSR at the Johns Hopkins University, Baltimore, MD 21218 USA (email: jhwu@mae.cuhk.edu.hk),

A. Related Work

Based on the different control methods, the robot systems can be divided broadly into either handheld, teleoperated, or cooperative-control robots [4]. A handheld robot is located between the surgeon's hand and the surgical instrument and is therefore directly manipulated by the surgeon. It represents the closest system to existing surgical methods and is the most intuitive for the surgeons to adopt. The Micron system of Carnegie Mellon University is the most famous handheld concept [5]. Micron uses a six-degree-of-freedom parallel mechanism driven by piezoelectric actuators to compensate for small movements and can realize the remote center of motion (RCM) movement around the sclera entry point.

A teleoperated system includes a robot close to the patient and a joystick (or other user interface) directly operated by the surgeon, which can achieve position scaling and hand tremor filtering. SMOS [6], Preceyes [7], and RAMS [8] robots are some of the well-known robotic systems in this field, with various RCM mechanisms. In recent years, researchers developed continuum robots, such as IRIS [9] from Johns Hopkins University, which expanded the freedom of manipulation of surgical instruments inside the eyeball.

A cooperative-control robot is defined as a robotic system that holds surgical instruments simultaneously with the surgeon. Using this type of system can preserve the traditional operating experience of most surgeons. An example of a cooperative-control system is the SHER from Johns Hopkins



Kong, HKSAR, and with LCSR at the Johns Hopkins University, Baltimore, MD 21218 USA (email: jhwu@mae.cuhk.edu.hk),

A. Alamdar, R. H. Taylor, I. Iordachita are with LCSR at the Johns Hopkins University, Baltimore, MD 21218 USA (aalamda3, rht, iordachita@jhu.edu)

P. Gehlbach is with the Wilmer Eye Institute, Johns Hopkins Hospital, Baltimore, MD 21287 USA (e-mail: pgelbach@jhmi.edu).

University [10]. The robotic systems of King's College London and Moorfields Eye Hospital [11], as well as KU Leuven [12] also belong to this category. Bilateral (also Bimanual) vitreoretinal micro-surgery, using two tools inside the eye, is considered essential in complex cases [13]-[15].

Previous research by Wu et al. [16] of our research group, showed that a four-bar linkage type tilt mechanism can achieve a good tradeoff between desired properties, such as hand space for surgeon control, small mechanism size and a small required linear movement range for compensating RCM motion. In the same work the authors generated two separately optimized four-bar mechanisms, yielding different results for the left-side and the right-side robot.

B. Novel approach

As compared to the previous optimization [16] of the tilt mechanism we are seeking a solution, which is equivalently applicable for the left-side robot (LSR) and the right-side robot (RSR) for a bilateral surgical approach towards the operated eye, while possessing a smaller range of compensation motion for enforcement of the V-RCM than the previous RSR result. The equivalence of the left and right robot design will support clinical introduction, provide flexibility in use, and will remain favorable with respect to design and control development. Furthermore, this approach could facilitate enhancement of safety by unifying the manipulation feeling of the surgeons and reducing the required range of compensation motions. To enable both adding the new constraints to the problem and improving the overall quality of the optimization result, we add detail in our cost function and introduce new freedoms. One such freedom is the use of a passive tilt support for the robot (Fig. 1, right). New freedoms are also gained by greater detail of representation, such as in the use of a patient safety space and surgeon hand space in the cost function to optimize for sufficient distance around the mechanism. The optimization is expanded to include the tilt resolution of the mechanism by adding the coupled slider-crank mechanism to the optimization and using the ratio of input to output velocity in the cost function. The mechanism weight, the corresponding arm moment, and the bending of the mechanism links are added to the cost function. These new parameters could improve the performance of the design. The shown optimization strategy, which considers not only kinematics, but also dynamics, stiffness, and ergonomics may be useful in the development of other cooperatively controlled robots.

II. OPTIMIZATION OF THE TILT MECHANISM

A. Design requirements and clinical setting

Fig. 2 shows the bilateral surgical approach in a transverse cross-section of the eye, also showing the face contour in this plane. A tool such as a needle, forceps or light-pipe is inserted through a trocar at the sclera entry point (red) and can be translated in insertion direction, tilted and rolled to reach the surgical site. A tilt range of 50° is assumed to be the workspace required during a procedure [12], [16]-[18] and is depicted in green. The home tilt (h) of the tool is defined by the line connecting the sclera entry point to the intersection point of vision axis and retina. From (h) we define a left and a right tilt, (l) and (r), at $\pm 25^\circ$ tilt. The placement of this 50° bilateral working range can be modified depending on the location of the surgical site, by choosing and planning a different initial

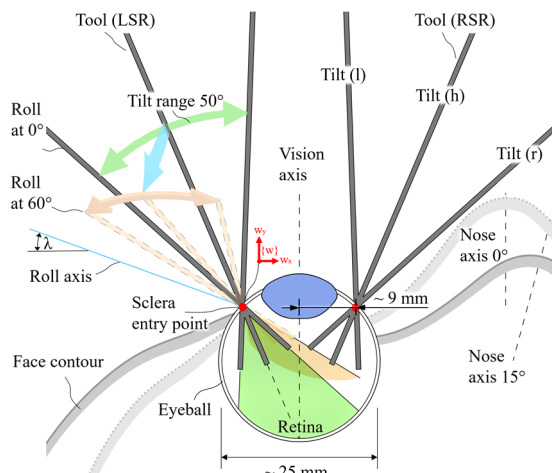


Figure 2. Tilt and roll in bilateral surgical approach

tilt of the robot arm with an adjustable passive arm fixture. The freedom for tool approach is however limited by the anatomy of the face, where the nose primarily impacts the RSR. By introducing an angle of approximately 15° between the nose axis and the vision axis of the patient, by head and eye rotation, this limitation can be reduced (see Fig. 2, Face contour). The position of the surgical microscope must also be considered. The roll axis of the tool may come in an angle λ towards the eye. It is shown in Fig. 2 for $\lambda = 20^\circ$ and depends on robot design as well as the chosen initial passive tilt. How roll around this axis affects the workspace is presented in orange (dashed outline) for a roll angle of 60° .

B. Description of tilt mechanism

The kinematic structure of the tilt mechanism that will be optimized is depicted in Fig. 3. Here, the joints A, B, C and D form a four-bar linkage mechanism. The joints A and B are fixed to the robot arm. This mechanism is actuated by an offset slider-crank mechanism with joints R, Q and A, where joint R is moved by a linear actuator. The rigid three-joint link QAD transfers the motion from the slider-crank to the four-bar. Furthermore, a tool-holder is mechanically fixed to the link CD and defines the offset towards the point P, which is the intended primary location for the RCM of the tool. As a four-bar mechanism cannot provide a real RCM, the point P will change its position in the robot arm coordinate system $\{a\}$ during tilting of the tool. As previously mentioned, this movement can be actively compensated with the degrees of freedom of the delta robot, hereby ensuring a V-RCM.

For the purposes of this study, we assume the robot roll axis of the SHER (Fig. 1) is parallel to the axis of linear actuation, as this choice is useful for the reduction of the

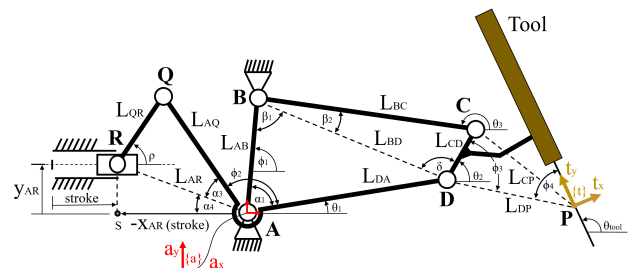


Figure 3. Mechanical structure of the tilt mechanism

moment of inertia of the robot arm. Furthermore, for simplicity of description, we introduce a coordinate frame $\{w\}$, where the vision axis, rather than the orientation of the ground, patient head or the robot arm, is chosen parallel to its y -axis (Fig. 2). The tilt mechanism for RSR and LSR should be symmetric to each other with respect to the vision axis, as asymmetry of approach, with different roll axis angles towards the vision axis, would only reduce the range of overlapping workspace for bilateral procedures. For further convenience, the origin of the coordinate frame $\{w\}$ is set at the sclera entry point.

C. Optimization method

A real-coded genetic algorithm (RCGA) [19],[20] was chosen for optimization, as this allows for a simple implementation, requires no calculation of intricate gradients and runtime is no primary concern. The genetic algorithm was realized using MATLAB (MathWorks, ver. R2020a). The problem was simplified to a 2D problem in the tilting plane, as the tilting mechanism is planar. Six vectors were used to describe the mechanism. They form the genes of each solution individual in the optimization. Considering each optimization parameter as a 2D vector rather than using two independent x and y parameters is useful for meaningful 2D crossover and mutation operators whose performance is independent from the used coordinate system [21]. The following vectors were used as gene parameters for the optimization.

$$\text{Individual}_i = \{\vec{C}_{\{t\}}, \vec{D}_{\{t\}}, \vec{P}_{l\{w\}}, \vec{P}_{r\{w\}}, \vec{Q}_{h\{w\}}, \vec{R}_{l\{w\}}\}, \quad (1)$$

where the vectors denote the locations of points of the mechanism structure (see Fig. 3). The joints C and D are described in the tool-fixed coordinate frame $\{t\}$ (Fig. 3), while the other vectors use the eye-fixed frame $\{w\}$ (Fig. 2). For vectors that depend on the configuration of the mechanism, the index l, h, r denotes that the point position is measured in the configuration corresponding to the tilt positions (l) , (h) , (r) of the tool (Fig. 2), respectively. The gene parameters allow flexibility, as a candidate mechanism might look quite different than the generic mechanical structure in Fig. 3. For instance, the joint A could also be above B giving a mechanism where the top link is driven.

As parent selection operator, we use proportionate selection [19], where individuals with lower cost are more likely to get selected as parents. The crossover of individuals is implemented similar to that of blending crossover BLX- α [20], while using a gaussian distribution $N(\mu, \sigma^2)$ instead of a bounded uniform distribution. For the crossover (2), (3) each 2D gene \vec{c}_1 and \vec{c}_2 of child₁ and child₂ are based on the difference between genes \vec{p}_1 and \vec{p}_2 of the selected parents. The parameters $\mu = 0.4$ and $\sigma = 0.2$ were chosen.

$$\vec{c}_1 = \vec{p}_1 + (\vec{p}_2 - \vec{p}_1) N(\mu, \sigma^2) \quad (2)$$

$$\vec{c}_2 = \vec{p}_2 + (\vec{p}_1 - \vec{p}_2) N(\mu, \sigma^2) \quad (3)$$

Gaussian mutation [21] of a child gene occurs with a certain probability. In this case a mutation vector is generated by a centered multivariate gaussian distribution, where the aggressiveness of search is adjusted by setting the variance. Therefore, the variance was reduced by a factor of 0.1 for the genes setting the position of P in (l) and (r) configurations, as it was observed that small changes hereof result in relatively large changes for the mechanism properties.

An Elitism [19] operator was used to prevent increasing cost of the best solution from one to the next generation, where a small fraction of the best solutions of the previous generation substitute the worst in the new population. Reiterating the algorithm with different randomized initial populations was used to provide an extensive search in the entire search space.

D. Cost function and constraints

An important part of the present optimization is the cost function, by which the quality of a candidate solution individual is calculated from its genes. Since the cost function C_{Total} should approximately reflect the complex nature of the real problem, it consists of the following subcategories:

$$C_{Total} = C_{RLM} + C_F + C_H + C_{Pos.Err.} + C_W + C_R \quad (4)$$

C_{RLM} : Firstly, we consider the required linear movements (RLM) for the mechanism to ensure a V-RCM. This part of the cost function is calculated using the forward kinematics (see Section E) and orthogonal projection of the resulting trajectory of point P on the a_x and a_y axis of the robot arm coordinate frame $\{a\}$. The cost of the RLM range in a_x , a_y and a_z direction is set at 1 per millimeter, where the range in a_z direction is equal to that in a_y , to account for movement during roll motion.

C_F : To calculate the distance of the tilt mechanism joints to the patient face, it is abstracted to only the contour-line of the face in the transversal plane of the eye (see Fig. 4). The minimum distance to the face is calculated for each joint in configurations (l) , (h) , (r) using the two different orientations of the face for LSR and RSR. In doing this, it is essential to consider the joint positions with added V-RCM compensation movement, as this will reflect the actual position of the joints during usage. The cost is calculated in 3 zones, where distance below 35 mm has a high penalty cost of 20 per millimeter below this boundary. A distance below 60 mm shows a lower priority preference with a cost of 2 per millimeter below 60 mm. Above 60 mm it is viewed as having no preference with a cost of zero. This safety distance to the patient's face is chosen to also allow for a certain flexibility of placement. Using a different tilt of the passive support is hereby possible for surgeries which do not use the full tilting workspace.

C_H : Similarly, a circle is defined to represent the surgeon's hand in the mechanism plane. This is illustrated in Fig. 4, where a circle of 30 mm radius is centered at an offset to the point P of -7 mm along the t_x axis and 50 mm along the t_y axis. A high penalty applies where the minimum joint distance to the circle center is under 32 mm with cost of 5 per millimeter below the boundary. The other zones are below 35 mm, with a cost of 0.5 per millimeter and zero cost above 35 mm.

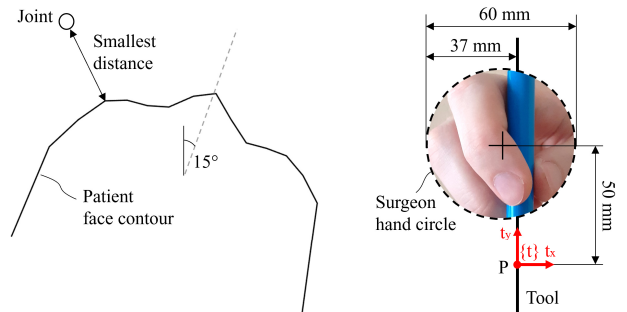


Figure 4. Patient face and surgeon hand abstractions

$C_{Pos,Err.}$: This part of the cost function contains a bending estimation for a worst-case force of 5 N that might be applied by a clinician in normal direction to the mechanism plane. It will also effectively work towards reducing the overall size of the mechanism. Calculations were based on a link cross-section with two segments of 5x10 mm, using the Young's modulus of Aluminum, and the length and height of the mechanism. Bending of the three-joint link QAD (Fig. 3) is intentionally neglected, as this could be easily prevented by a design with large cross-section, while bending is not so easily preventable near the link BC towards the inside of the four-bar mechanism, as this is where the force/torque sensor should be placed in the design. 1 μm displacement is set to be equivalent to a $C_{Pos,Err.}$ cost increase of 1. Another part of $C_{Pos,Err.}$ is the amplification of unwanted displacements at the delta robot. Assuming a deformation causing angulation of the arm of 1 μm per 30 mm of the arm length, we correspondingly consider an additional cost of 1 per 30 mm length of the tilt mechanism. Finally, we also take a closer look at link QAD to consider the amplification factor for unwanted displacements (e.g. bushing deformation or play) in the joint Q of the mechanism. Assuming 1 μm displacement at Q we can estimate the additional cost directly with the ratio L_{DA}/L_{AQ} .

C_W sets a cost on the link lengths to reduce the size and weight of the mechanism. We can also introduce a penalty for unreasonably tall mechanism fixtures for joints A or B. As presented in (5), C_W is based on the sum of all link lengths L_{Links} an estimation of the minimum fixture design height h_F which is the offset between the actuator base and one fixture joint A or B, and contains a consideration of the maximum moment based on mechanism mass. The factor of 3 is introduced to account for the more rigid design of the fixture that is expected as compared to that of the links. M_{max} is the maximum moment in configurations (l), (h), (r) based on mechanism weight and the lever arm of the mechanism center of mass as measured towards the center of the delta robot at ~ 150 mm from the stroke starting position. For this we use the density of Aluminum and the link cross-section in two segments of 5x10 mm. Increasing the length of one link by 1 mm in L_{Links} is set at an equal cost as increasing M_{max} by 1 Nmm.

$$C_W = \frac{1}{15} (L_{Links} + 3 h_F + M_{max}) \quad (5)$$

C_R : The cost C_R contains multiple considerations to determine if the mechanism is realizable. Using high penalties, it deals with unsolvable mechanisms, mechanism singularities, minimum joint angles and minimum link lengths and makes sure the joints lie below the tool axis in each configuration so that the mechanism does not interfere with the microscope vision. Intersections between links are not restricted, as it is likely there will still be a possible design solution in 3D space. Likewise, links were also intentionally not considered in hand space and face space calculations, as links do not have to be linear and could be easily curved in design to prevent such issues. Besides the mentioned components, the realizability cost imposes a penalty on the passive tilt angle of 1 per 1.5 degrees. Similarly, the perpendicular offset between the line of the actuator base and the sclera point should also be kept small enough, which can be achieved by imposing a penalty cost of 1 per 5 mm offset. Finally, we need to maintain a good resolution for the tilting motion given the input resolution of the linear actuator (KR15, THK, Japan, 50mm Stroke,

precision grade). With the forward kinematics for the general mechanism (Section E), we calculate the ratio of the input stroke velocity to the output tilt angle velocity of the mechanism, which is a variable of the input stroke position s .

$$VelocityRatio(s) = \frac{d\theta_{Tool}(s)}{ds} \quad (6)$$

The related cost increase is 4 times the maximum velocity ratio divided by the average ratio.

E. Forward kinematics

The forward kinematics for the general mechanical structure of the tilt mechanism (see Fig. 3) is calculated as follows. Choosing a linear actuator with a stroke length of 50mm, we have $s \in [0, 50]$.

$$x_{AR}(s) = x_{AR}(0) \pm s \quad (7)$$

where \pm is positive for a mechanism with left to right stroke.

$$L_{AR} = \sqrt{x_{AR}^2 + y_{AR}^2} \quad (8)$$

$$Sign_{alpha3} = \text{Sign}(\overrightarrow{AR}_x \overrightarrow{AQ}_y - \overrightarrow{AR}_y \overrightarrow{AQ}_x) \quad (9)$$

$Sign_{alpha3}$ is used to express the two possible solutions for α_3 corresponding to the side of the diagonal AR that Q is at.

$$\alpha_3 = \arccos\left(\frac{L_{AR}^2 + L_{AQ}^2 - L_{QR}^2}{2L_{AR}L_{AQ}}\right) Sign_{alpha3} \quad (10)$$

$$\alpha_4 = 180^\circ - \arctan2(y_{AR}, x_{AR}), \quad (11)$$

where the $\arctan2(y,x)$ function is the four-quadrant inverse of the tangent function, which is equal to the counterclockwise Euclidean angle for a vector $[x; y]$ and has an implementation as a standard library function in MATLAB.

$$\theta_1 = 180^\circ - (\varphi_2 + \alpha_3 + \alpha_4) \quad (12)$$

$$\alpha_1 = \varphi_1 - \theta_1 \quad (13)$$

$$L_{BD} = \sqrt{L_{AB}^2 + L_{DA}^2 - 2L_{AB}L_{DA} \cos \alpha_1} \quad (14)$$

$$\beta_1 = \arccos\left(\frac{L_{AB}^2 + L_{BD}^2 - L_{DA}^2}{2L_{AB}L_{BD}}\right) Sign(\alpha_1), \quad (15)$$

where α_1 ranges between -180° and 180° .

$$Sign_{delta} = \text{Sign}(\overrightarrow{DC}_x \overrightarrow{DB}_y - \overrightarrow{DC}_y \overrightarrow{DB}_x) \quad (16)$$

$Sign_{delta}$ is used to express the two possible solutions for δ corresponding to the side of the diagonal BD that C is at.

$$\delta = \arccos\left(\frac{L_{CD}^2 + L_{BD}^2 - L_{BC}^2}{2L_{CD}L_{BD}}\right) Sign_{delta} \quad (17)$$

$$\theta_2 = \varphi_1 + \beta_1 - \delta \quad (18)$$

Finally, we have the transformation matrix from coordinate frame $\{a\}$ to $\{t\}$.

$$\mathbf{T}_D^{\{a\}} = \text{Rot}(a_z, \theta_1) \text{Trans}(a_x, L_{DA}) \quad (19)$$

$$\mathbf{T}_P^D = \text{Rot}(a_z, \theta_2 - \varphi_3 - \theta_1) \text{Trans}(a_x, L_{DP}) \quad (20)$$

$$\mathbf{T}_{\{t\}}^{\{a\}} = \mathbf{T}_D^{\{a\}} \mathbf{T}_P^D \text{Rot}(a_z, 90^\circ - \varphi_4 - (\theta_2 - \varphi_3 - \theta_1)) \quad (21)$$

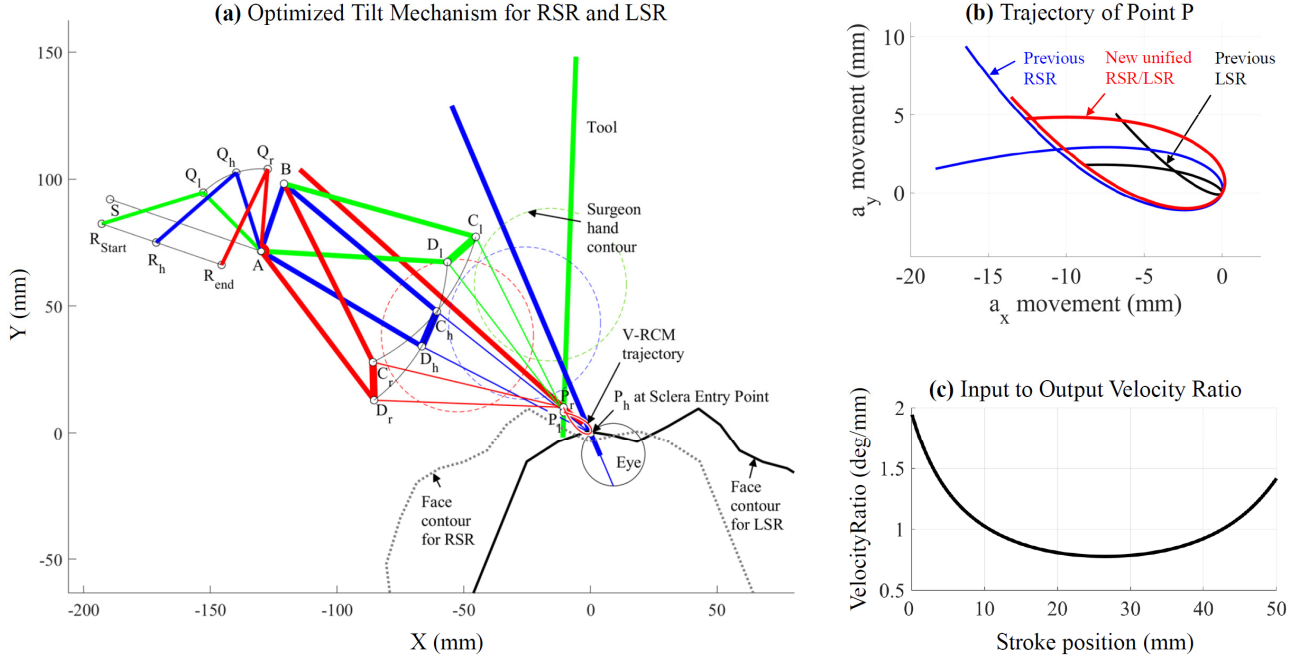


Figure 5. (a) Mechanism result in configurations (*l*), (*h*), (*r*) with face contours for LSR and RSR approach, (b) Trajectory of point P during tilt as compared to that of previous RSR and LSR optimization results, (c) Input to output velocity ratio

F. Optimization Result

The optimized tilt mechanism is shown in Fig. 5a, in (*l*), (*h*) and (*r*) configuration, where the optimized gene vectors (see (1)) are $\{[-37.10; 67.78], [-47.93; 57.45], [-10.56; 8.22], [-10.65; 10.15], [-139.77; 102.53], [-192.86; 82.39]\}$. From the optimized solution we can derive the following design parameters:

$$\begin{aligned} L_{AB} &= 28 \text{ mm}, L_{BC} = 78.5 \text{ mm}, L_{CD} = 15 \text{ mm}, \\ L_{DA} &= 73.5 \text{ mm}, L_{AQ} = 32.5 \text{ mm}, L_{QR} = 42 \text{ mm}, \\ L_{CP} &= 77.3 \text{ mm}, L_{DP} = 74.8 \text{ mm}, \\ x_{AR} &= -63 \text{ mm}, y_{AR} = -10 \text{ mm}, \phi_1 = 90^\circ, \phi_2 = 138^\circ. \end{aligned}$$

Here, the offset between the actuator base and the roll axis is 15.5 mm. The passive tilt of the linear actuator base is 18.9° relative to a plane perpendicular to the vision axis. This allows for a placement of the 50° tilt range as shown in Fig. 2. Furthermore, the angles α_3 and δ remain positive. Fig. 5b shows the movement of the tool RCM, where a vector from a curve point to the origin of the diagram corresponds to the RLM to ensure the virtual-RCM. Here, it can be observed that the optimized tilt mechanism, which is the result of this paper, has RLM values that are in-between the previous optimizations for different LSR and RSR by Wu et al. [16].

The size comparison of the total range for the RLM, which must be provided by the delta robot of the SHER, is presented in Table 1. Fig. 5c represents the input to output velocity ratio of the optimized mechanism. With this, we can calculate a theoretical resolution and backlash of the tilting motion based on that of the linear actuation by rearranging (5). Using the maximum velocity ratio of ~ 2 deg/mm, a displacement of 1 μm at the linear stage results in a tool tilt of 0.002° which is

equivalent to 0.000035 rad. The nominal repeatability of the used linear stage is $\pm 3 \mu\text{m}$, similarly giving ± 0.0001 rad.

TABLE I. REQUIRED LINEAR COMPENSATION MOVEMENTS

RLM range for V-RCM compensation in mm	Comparison with previous optimization		
	Previous LSR [16]	New unified RSR/LSR	Previous RSR [16]
RLM in a _x direction	8.77	13.72	18.90
RLM in a _y direction	5.08	7.15	10.50

III. DESIGN AND VERIFICATION OF THE TILT MECHANISM

In order to verify the applicability of the optimization result, a corresponding mechanism design was created. The whole robot was 3D-printed and assembled, where important parts such as the Linear stage (KR15, THK, Japan) and the Force-Torque sensor (Nano17, ATI, USA) were added.

To imitate the surgical setup, a medical phantom (SKU 1345-18-1, Sawbones, USA) was placed on a table under a surgical microscope. In two parts of the experiment, the robot prototype was fixed to the table, either on the left or right of the patient where the applicability as LSR and as RSR could be tested. The passive support used in the experiments is adjustable to set the passive tilt and passive yaw angles as defined in Fig. 6a. During the verification experiment the yaw angle of the passive support is set to +20°, 0° and -20° for the LSR and RSR cases. For each of these positions, the tilt mechanism was moved near both extreme configurations (*l*) and (*r*). The passive tilt angle of the support was set to 0° for LSR and $\sim 20^\circ$ for RSR. Head tilt and eye tilt were not adjusted in the experiments. Although, the lack of head tilt accentuates the anatomical constraints, the mechanism did not interfere with the patient anatomy. In an extreme case for LSR shown

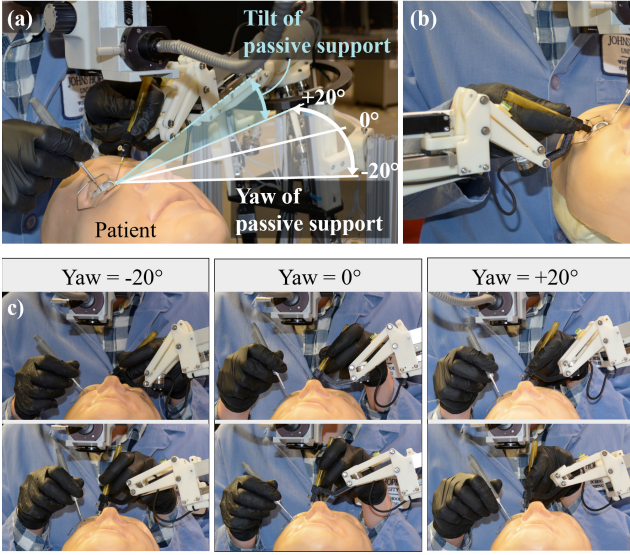


Figure 6. (a) Angles in verification experiment, (b) LSR at $+20^\circ$ yaw angle and 0° passive tilt at full insertion depth, (c) Yaw angles for RSR, where top and bottom images show extreme positions of the mechanism

in Fig. 6b, with $+20^\circ$ at the full insertion depth of the tool, we observe that the tilt mechanism (white) is still at a safe distance. From the same image it is apparent that the basic preliminary design of the tool-holder (Black part between tool and tilt mechanism, see also Fig. 1) comes close to the face at the full insertion depth of the tool. In Fig. 6c, it can be observed that the mechanism does not interfere with the patient anatomy.

Finally, for both RSR and LSR, the hand space was deemed sufficient, allowing a two-finger grip as well as a three-finger grip. The hand poses at a yaw angle of -20° and 0° were considered more ergonomic than those at $+20^\circ$.

IV. DISCUSSION

As presented in the results section, the optimization was able to reach a smaller RLM compared with the results reported in the previous work [16] despite the added constraints by optimizing a single mechanism for both sides. The anatomical constraints posed by the approach of the RSR are more challenging than those for the LSR side, due to the additional proximity to the nose and anatomy under the RSR. Notably, the new mechanism has a smaller RLM than that of the previous one-sided optimization for the RSR, which shows the newly introduced freedoms, including the higher detail of description in the optimization, have enabled an improved solution for the RSR. For the less challenging approach on the LSR side, the new mechanism still performs well, with an acceptable increase of RLM as compared to the previous one-sided optimization of the LSR. In the unfavorable case of a non-unified design, the new optimization could easily be modified to use only constraints of the LSR and would likely achieve a smaller RLM for the LSR than the previous work. Having a unified design is deemed more useful than a one-sided reduction of the RLM by 5 mm in a_x and 2 mm in a_y direction. Especially, since a mechanism, which is different for LSR and RSR would either give two different delta robot designs or would not enable reducing the size of the delta robot.

The new unification of the LSR and RSR design is expected to have several advantages including the ease in clinical use. Notably, the robots do not need to be switched between left eye and right eye surgeries. Moreover, the alternative use of a single SHER is more feasible with the new unified design, where the other side of the bilateral approach could be a traditional tool requiring less precision such as a light-pipe. This would also facilitate the clinical introduction for use in the intended two robot case. Having a unified SHER system may have a positive effect on surgeon training, reducing robot costs and robot maintenance is simplified. From a development perspective the design, manufacturing and control of the robot can also be unified.

A shorter robot arm might be beneficial to reduce errors by reducing deformations and the error amplification over longer distance. In considering the use of a shorter linear actuator with a modified optimization it would be imperative to consider the resulting tilt resolution, as shorter actuators would need a higher resolution to give the same tilt resolution, while also increasing the importance of rigidity and the reduction of play for the mechanism. For shorter stroke lengths, it also might be reasonable to allow for stroke directions that are not parallel to the roll axis. However, a shorter robot arm could introduce new issues for the positioning of the delta robot.

Our verification experiments demonstrate that the presented optimized tilt mechanism provides improved freedom of placement for clinical use. It is reasonable to suggest that this freedom could be further increased by also optimizing the tool-holder design. By eliminating interference with the patient, at the lowest anatomically feasible approach angle of the tool, the reachable workspace approaches or equals that of manual surgical procedures. However, at this time placement of the momentary 50° tilting range must still be planned. If a larger range is required during a particular surgery, additional reorienting of the initial passive tilt of the robot remains a requirement.

V. CONCLUSION

The following key points have been established:

- A tilt mechanism was optimized for use in robot-assisted vitreoretinal surgery systems, which is applicable equally to both robots during a bilateral surgical approach.
- A detailed cost function has been shown to present the tradeoff between multiple desirable properties of the tilt mechanism.
- The compensation range to enforce the virtual-RCM could be reduced compared with the results of the previous optimization by Wu et al. [16], despite using the constraints of both LSR and RSR.
- The resulting hand space for the surgeon was found to be sufficient, by verification in multiple directions of approach, for the extreme positions of the tilt mechanism.

Future work will be focused on calibration of the built mechanism and assessment of repeatability, resolution, and rigidity.

REFERENCES

- [1] T. Leng, J. M. Miller, K. V. Bilbao, D. V. Palanker, P. Huie, and M. S. Blumenkranz, "The chick chorioallantoic membrane as a model tissue for surgical retinal research and simulation," *Retina*, vol. 24, no. 3, pp. 427–434, 2004.
- [2] T. Rim, Y. Choi, S. Kim, M. Kang, J. Oh, S. Park, and S. Byeon, "Retinal vessel structure measurement using spectral-domain optical coherence tomography," *Eye*, vol. 30, no. 1, p. 111, 2016.
- [3] C. N. Riviere and P. S. Jensen, "A study of instrument motion in retinal microsurgery," in *Proceedings of the 22nd Annual International Conference of the IEEE Engineering in Medicine and Biology Society (Cat. No. 00CH37143)*, vol. 1. IEEE, 2000, pp. 59–60.
- [4] E. Vander Poorten, C. N. Riviere, J. J. Abbott, C. Bergeles, M. A. Nasseri, J. U. Kang, R. Sznitman, K. Faridpooya and I. Iordachita, "Robotic Retinal Surgery," in *Handbook of Robotic and Image-Guided Surgery*: Elsevier, 2020, pp. 627–672.
- [5] S. Yang, R. A. MacLachlan, and C. N. Riviere, "Manipulator design and operation of a six-degree-of-freedom handheld tremor-canceling microsurgical instrument," *IEEE/ASME transactions on mechatronics*, vol. 20, no. 2, pp. 761–772, 2014.
- [6] A. Guerrouad and P. Vidal, "Smos: stereotaxical microtelemanipulator for ocular surgery," in *Images of the Twenty-First Century. Proceedings of the Annual International Engineering in Medicine and Biology Society*. IEEE, 1989, pp. 879–880.
- [7] T. Meenink, G. Naus, M. de Smet, M. Beelen, and M. Steinbuch, "Robot assistance for micrometer precision in vitreoretinal surgery," *Investigative ophthalmology & visual science*, vol. 54, no. 15, pp. 5808–5808, 2013.
- [8] M. A. Nasseri, M. Eder, S. Nair, E. Dean, M. Maier, D. Zapp, C. P. Lohmann, and A. Knoll, "The introduction of a new robot for assistance in ophthalmic surgery," in *2013 35th Annual International Conference of the IEEE Engineering in Medicine and Biology Society (EMBC)*. IEEE, 2013, pp. 5682–5685.
- [9] J. Song, B. Gonenc, J. Guo, and I. Iordachita, "Intraocular snake integrated with the steady-hand eye robot for assisted retinal microsurgery," in *2017 IEEE International Conference on Robotics and Automation (ICRA)*. IEEE, 2017, pp. 6724–6729.
- [10] X. He, D. Roppenecker, D. Gierlach, M. Balicki, K. Olds, P. Gehlbach, J. Handa, R. Taylor, and I. Iordachita, "Toward clinically applicable steady-hand eye robot for vitreoretinal surgery," in *ASME 2012 international mechanical engineering congress and exposition*. American Society of Mechanical Engineers Digital Collection, 2012, pp. 145–153.
- [11] A. Mablekos-Alexiou, S. Ourselin, L. Da Cruz, and C. Bergeles, "Requirements based design and end-to-end dynamic modeling of a robotic tool for vitreoretinal surgery," in *2018 IEEE International Conference on Robotics and Automation (ICRA)*. IEEE, 2018, pp. 135–141.
- [12] A. Gijbels, N. Wouters, P. Stalmans, H. Van Brussel, D. Reynaerts, and E. Vander Poorten, "Design and realisation of a novel robotic manipulator for retinal surgery," in *2013 IEEE/RSJ International Conference on Intelligent Robots and Systems*. IEEE, 2013, pp. 3598–3603.
- [13] I. H. Fine, R. S. Hoffman, and M. Packer, "Optimizing refractive lens exchange with bimanual microincision phacoemulsification," *Journal of cataract and refractive surgery*, vol. 30, no. 3, pp. 550–554, 2004
- [14] H. C. Park, C. B. Yeo, P. L. Gehlbach, and C. Song, "Development of the dual SMART micro-surgical system using common-path swept source optical coherence tomography," *Annual International Conference of the IEEE Engineering in Medicine and Biology Society. IEEE Engineering in Medicine and Biology Society. Annual International Conference*, vol. 2015, pp. 5–8, 2015
- [15] D. Koo, H.-C. Park, P. L. Gehlbach, and C. Song, "Development and preliminary results of bimanual smart micro-surgical system using a ball-lens coupled OCT distance sensor," *Biomedical optics express*, vol. 7, no. 11, pp. 4816–4826, 2016
- [16] J. Wu, G. Li, M. Urias, N. A. Patel, Y. Liu, P. Gehlbach, R. H. Taylor, and I. Iordachita, "An Optimized Tilt Mechanism for a New Steady-Hand Eye Robot," in *2020 IEEE/RSJ International Conference on Intelligent Robots and Systems*. IEEE, 2020, pp. 3105–3111.
- [17] C.-Y. He, L. Huang, Y. Yang, Q.-F. Liang, and Y.-K. Li, "Research and Realization of a Master-Slave Robotic System for Retinal Vascular Bypass Surgery," *Chin. J. Mech. Eng.*, vol. 31, no. 1, 2018
- [18] Y. Ida, N. Sugita, T. Ueta, Y. Tamaki, K. Tanimoto, and M. Mitsuishi, "Microsurgical robotic system for vitreoretinal surgery," *International journal of computer assisted radiology and surgery*, vol. 7, no. 1, pp. 27–34, 2012
- [19] J. Kacprzyk, G. C. Onwubolu, and B. V. Babu, Eds., *New Optimization Techniques in Engineering*. Berlin, Heidelberg: Springer Berlin Heidelberg, 2004.
- [20] F. Herrera, M. Lozano, and A. M. Sánchez, "A taxonomy for the crossover operator for real-coded genetic algorithms: An experimental study," *Int. J. Intell. Syst.*, vol. 18, no. 3, pp. 309–338, 2003.
- [21] Y. Yoon and Y.-H. Kim, "The Roles of Crossover and Mutation in Real-Coded Genetic Algorithms," in *Bio-Inspired Computational Algorithms and Their Applications*, S. Gao, Ed.: InTech, 2012.